RSC Advances

PAPER

View Article Online
View Journal | View Issue

Cite this: *RSC Adv.*, 2022, **12**, 28137

3-(4-Formylphenyl)-triazole functionalized coumarins as violet-blue luminophores and n-type semiconductors: synthesis, photophysical, electrochemical and thermal properties†

José Emilio de la Cerda-Pedro, [ae] Oscar J. Hernández-Ortiz, [b] Rosa A. Vázquez-García, [b] Heraclio López-Ruiz,[c] Ramón Gómez-Aguilar, [d] Norberto Farfán [e] and Itzia I. Padilla-Martínez *[a]

Received 24th May 2022
Accepted 24th September 2022

DOI: 10.1039/d2ra03266j

rsc.li/rsc-advances

3-(4-Formylphenyl)-triazole-coumarin hybrid chromophores (FPhTCs) were synthesized in good yields, using a click chemistry protocol, and were also structurally characterized. Their photophysical, electrochemical and thermal properties were measured demonstrating that FPhTCs are luminescent in the blue-violet region of the electromagnetic spectrum, both in solution and the solid state. They showed an electrochemical band-gap values of 2.79 ± 0.08 eV, resistivity values between 10^4 and 10^5 Ω cm and are thermally stable up to 225 °C, properties that promise FPhTCs as good candidates for optoelectronic or imaging applications. Their solution and solid state photoluminescent properties are discussed and supported by theoretical calculations.

1 Introduction

The study and applications of the photophysical and semiconductor properties of small-organic (SO) molecules has become an important area of research. In the last two decades, numerous organic compounds with a wide spectrum of photophysical properties have been developed allowing a better understanding of the relationship between structural features and photophysical properties.[1] SO fluorophores are pure compounds of well-known structures with relatively low production costs, whose structures are easily modified to obtain tunable photophysical properties. In this regard, SO fluorophores have been used for bioimaging applications,[2,3] organic optoelectronics[4] and organic light-emitting diodes (OLEDs).[5,6] The violet-blue luminescence is very important in OLEDs, as one of the three primary colors for white light generation.[7] In addition, promising applications in high-density information storage[8] and biological photo-inactivation,[9] among others, have also been reported.

In this context, coumarin and its derivatives are privileged structures with exceptional optical properties. They are considered as extremely efficient fluorophores with large Stokes shift values, high quantum yields and high photostability.[10] Therefore, they have been applied as emission layers in organic light-emitting diodes (OLED),[11] fluorescent dyes and probes,[12,13] and nonlinear optical chromophores. On the other hand, 1,2,3-triazoles are well known blue emitting chromophores, with applications as photostable fluorescent brightening agents, metal sensors, materials for optoelectronic devices, donor–acceptor chromophores[14] and chemosensors.[15] Because of their optical properties, triazoles have been used as fluorescent linkers between two or more molecular fragments, showing an ambipolar behavior, depending on the substitution position.[16] The 1,2,3-triazole ring has been incorporated as a 3-, 4-, 5- and 7-substituent into the coumarin heterocycle, acting as a linker between coumarin and other heterocycles,[17–19] glycosides,[20,21] polymeric chains;[22] or a phenyl ring.[23,24] All these SO conjugates share the non-planarity as a common feature through the incorporation of C(sp^3) or O(sp^3) atoms as part of the linker to improve solubility.

[a]*Laboratorio de Química Supramolecular y Nanociencias de la Unidad Profesional Interdisciplinaria de Biotecnología del Instituto Politécnico Nacional, Av. Acueducto s/n Barrio la laguna Ticomán, Ciudad de México, 07340, Mexico. E-mail: ipadillamar@ipn.mx*

[b]*Área Académica de Ciencias de la Tierra y Materiales, Universidad Autónoma del Estado de Hidalgo, km. 4.5 Carretera Pachuca-Tulancingo, Col. Carboneras, Mineral de la Reforma, Hidalgo, 42184, Mexico*

[c]*Área Académica de Química, Universidad Autónoma del Estado de Hidalgo, km. 4.5 Carretera Pachuca-Tulancingo, Col. Carboneras, Mineral de la Reforma, Hidalgo, 42184, Mexico*

[d]*Unidad Profesional en Ingeniería y Tecnologías Avanzadas del Instituto Politécnico Nacional, Av. I.P.N No. 2580 Col. La Laguna Ticomán, Gustavo A. Madero, Ciudad de México, 07340, Mexico*

[e]*Facultad de Química, Departamento de Química Orgánica, Universidad Nacional Autónoma de México, Circuito Escolar, Ciudad Universitaria 04510, Ciudad de México, Mexico*

† Electronic supplementary information (ESI) available. See https://doi.org/10.1039/d2ra03266j

In contrast, as part of a full delocalized system, 1,2,3-phenyltriazolyl-coumarins have been synthesized incorporating substituents in both the coumarin heterocycle and in the phenyl ring with the purpose of increasing the fluorescence.[25,26] Recently, our group has also reported the fluorescent properties of 3-phenyl-triazolyl-coumarins in the context of crystal engineering.[27] Nevertheless, it is known that electron-donor (ED) substituents on C-7 and electron-withdrawing (EW) substituents on C-3 lead to push–pull systems in the coumarin structural unit, inducing a strong polarization that allows tuning their absorption-emission profiles.[28] In addition, SO conjugates of triazole (T) and coumarin (C) moieties are also known to possess improved optical properties tuned by the position and nature of the coumarin substituents.[25,29] Although the study of coumarin functionalization and its impact on their optical properties has been reported, the molecular structures of coumarins are varied and diverse.[30] Coumarin derivatives have exhibited attractive applications in solar cells[31,32] and as fluorescent chemosensors although with relatively low quantum yields[33] and in some cases exhibiting AIE (aggregation induced emission) with potential use in bioimaging.[34] Herein, 3-(4-formylphenyl)triazolyl-coumarin (FPhTC) conjugates **1a–g** have been synthesized with the aim of establishing a structure–property relationship of the coumarin substitution and the role of triazole on the photophysical properties of this molecular scaffold. With this, knowledge is provided in the rational design of π-conjugated systems derived from coumarins with potential application in optoelectronics. The synthesis was performed in one step; the compounds were spectroscopically, spectrometric and thermally characterized. Finally, their photophysical and electrochemical properties were explored and supported by mechano-quantum calculations.

2 Experimental

2.1 Materials and methods

All reagents were purchased from Sigma-Aldrich. Organic solvents were dried by standard procedures. Melting points were determined with a Electrothermal AI 9100 apparatus and are uncorrected. FT-IR spectra were recorded on a PerkinElmer Spectrum GX Spectrophotometer and are reported in terms of frequency of absorption (cm^{-1}). ^1H and ^{13}C chemical shifts, were acquired on Varian NMR spectrometers, operating at 300, 400 or 750 MHz using DMSO-d_6 or $CDCl_3$ as solvents. All chemical shift values (δ) are reported in parts per million (ppm), using as reference the residual solvent peak ($CDCl_3$: ^1H, δ 7.26; ^{13}C, δ 77.16; DMSO-d_6: ^1H, δ 2.50; ^{13}C, δ 39.52) and coupling constants (^nJ) are in Hz. To indicate the multiplicity of the signals, the following abbreviations are used: s, for a singlet; d, for a doublet; dd, for a doublet of doublets; t, for a triplet; q, for a quadruplet; m, for multiplet, or different combinations of the above. High resolution mass spectra were obtained with an Agilent G1969A spectrometer. The UV-vis and emission spectra were recorded with a PerkinElmer Lambda XLS spectrophotometer and PerkinElmer LS55 fluorescence spectrometer, respectively, using 1 cm path length cuvettes of quartz at room temperature. Thin films were supported on a quartz surface by immersion during 40–50 min in CH_2Cl_2 solutions of **1a–g** (2×10^{-4} M, 290 nm), for absorption and emission measurements. DSC and TG measurements were performed in a Q2000 equipment and a Thermobalance Q5000 IR, respectively, of TA instruments. In both cases, approximately 3.0–5.0 mg of sample was used and a gradient of 5.0 °C min^{-1} from room temperature to 350 °C under air flux of 25 mL min^{-1} in an open (TG) or pin-holed panels (DSC).

2.2 General procedure for the synthesis of 1,2,3-triazolyl-phenyl-coumarin hybrids (PFhTCs 1a–g)

A four-component one pot methodology reported elsewhere was followed,[27] starting from the corresponding salicylaldehydes, ethyl bromoacetate, 4-ethynylbenzaldehyde and sodium azide under mild conditions, but using CuCN (10% equiv.) as catalyst instead of CuI. After the refluxing period, 20 mL of cold MeOH–H_2O mixture (1 : 3 v/v) was added instead of AcOEt used in the original procedure. The solid was filtered and washed with the same mixture to obtain the final products. ^1H, ^{13}C and high-resolution mass spectra (HRMS) of compounds **1a–g** are shown in Fig. S1–S21.†

2.2.1 4-(1-(2-oxo-2*H*-chromen-3-yl)-1*H*-1,2,3-triazol-4-yl) benzaldehyde (1a). White crystalline solid (87%). Mp: 269–271 °C. ^1H NMR (400 MHz, DMSO-d_6, δ): 10.01 (s, 1H, HCO), 9.25 (s, 1H, H-9), 8.78 (s, 1H, H-4), 8.12 (d, 2H. ^3J = 8.2, H-13), 8.01 (d, 2H, ^3J = 8.2, H-12), 7.95 (dd, 1H, ^4J = 1.2, ^3J = 7.6, H-5), 7.74 (td, 1H, ^4J = 1.2, ^3J = 7.6, H-7), 7.55 (d, 1H, ^3J = 7.9, H-8), 7.47 (t, 1H, ^3J = 7.6, H-6). ^{13}C NMR (100.6 MHz, $CDCl_3$, δ in ppm): 191.6 (HCO), 167.7 (C-2), 155.8 (C-8a), 152.7 (C-10), 136.1 (C-7), 133.2 (C-14), 133.0 (C-11), 132.5 (C-5), 130.9 (C-4), 130.5 (C-13), 129.1 (C-3), 128.8 (C-6), 126.3 (C-12), 125.8 (C-9), 121.7 (C-8), 116.8 (C-4a). FT-IR (cm^{-1}): 3156, 2112, 1722, 1699, 1612, 1464, 1220, 819, 773. HR-MS (ESI-TOF) m/z calcd for $C_{18}H_{11}N_3O_3$ $[M + H]^+$: 318.0873, found 318.0874.

2.2.2 4-(1-(6-Methoxy-2-oxo-2*H*-chromen-3-yl)-1*H*-1,2,3-triazol-4-yl)benzaldehyde (1b). White crystalline solid (97%). Mp: 266–268 °C. ^1H NMR (400 MHz, $CDCl_3$, δ in ppm): 10.05 (s, 1H, HCO), 9.09 (s, 1H, H-9), 8.66 (s, 1H, H-4), 8.12 (d, 2H, ^3J = 8.3, H-13), 7.99 (d, 2H, ^3J = 8.3, H-12), 7.40 (d, 1H, ^3J = 9.1, H-8), 7.24 (dd, 1H, ^3J = 9.1, ^4J = 2.9, H-7), 7.11 (d, 1H, ^4J = 2.9, H-5), 3.91 (s, 3H, CH_3). ^{13}C NMR (100.6 MHz, $CDCl_3$, δ): 191.6 (HCO), 157.0 (C-6), 155.9 (C-2), 147.2 (C-8a), 146.8 (C-10), 136.1 (C-14), 135.8 (C-11), 133.0 (C-4), 130.5 (C-13), 126.3 (C-12), 121.7 (C-3), 121.2 (C-9), 121.1 (C-7), 118.5 (C-4a), 117.9 (C-8), 110.4 (C-5), 55.9 (CH_3). FT-IR (cm^{-1}): 3164, 1724, 1690, 1573, 1428, 1315, 1144, 1062. HR-MS (ESI-TOF) m/z calcd for $C_{19}H_{13}N_3O_4$ $[M + H]^+$: 348.0978, found 348.0979.

2.2.3 4-(1-(7-(Diethylamino)-2-oxo-2*H*-chromen-3-yl)-1*H*-1,2,3-triazol-4-yl)benzaldehyde (1c). Brown crystalline solid (75%). Mp: 245–247 °C. ^1H NMR (400 MHz, $CDCl_3$, δ):10.04 (s, 1H, HCO), 8.96 (s, 1H, H-9), 8.49 (s, 1H, H-4), 8.10 (d, 2H, ^3J = 8.0, H-13), 7.96 (d, 2H, ^3J = 8.0, H-12), 7.46 (d, 1H, ^3J = 8.8, H-5), 6.74 (dd, 1H, ^3J = 8.8, H-6), 6.62 (s, 1H, H-8), 3.47 (q, 4H, ^3J = 7.2, CH_2), 1.27 (t, 6H, ^3J = 7.2, CH_3). ^{13}C NMR (100.6 MHz, $CDCl_3$, δ): 191.7 (HCO), 156.8 (C-2), 155.8 (C-7), 151.3 (C-10), 146.3 (C-8a), 136.3(C-14), 135.9 (C-11), 134.5 (C-4), 130.4 (C-13), 130.2 (C-5), 126.2 (C-12), 121.5 (C-9), 116.9 (C-3), 110.6 (C-6), 107.5 (C-4a),

97.6 (C-8), 45.4 (CH_2), 12.3 (CH_3). FT-IR (ATR, cm^{-1}): 3067, 1745, 1678, 1522, 1145, 1031. HR-MS (ESI-TOF) *m*/*z* calcd for $C_{22}H_{20}N_4O_3$ $[M + H]^+$: 389.1608, found 389.1606.

2.2.4 4-(1-(6-Bromo-2-oxo-2*H*-chromen-3-yl)-1*H*-1,2,3-triazol-4-yl)benzaldehyde (1d). Beige solid (93%). Mp: 285–286 °C. ^{1}H NMR (300 MHz, DMSO-d_6, δ):10.04 (s, 1H, HCO), 9.30 (s, 1H, H-9), 8.77 (s, 1H, H-4), 8.23 (m, 3H, H-5, H-13), 8.03 (d, 2H, $^3J = 8.2$, H-12), 7.90 (dd, 1H, $^4J = 2.3$, $^3J = 9.0$, H-7), 7.56 (d, 1H, $^3J = 9.0$, H-8). ^{13}C NMR (75.4 MHz, DMSO-d_6, δ):193.1 (HCO), 155.8 (C-2), 149.5 (C-8a), 146.1 (C-10), 139.3 (C-7), 136.2 (C-14), 135.9 (C-11), 134.1 (C-4), 131.9 (C-5), 130.9 (C-13), 126.5 (C-12), 124.4 (C-3), 124.0 (C-9), 120.7 (C-6), 119.1 (C-8), 117.4 (C-4a). FT-IR (cm^{-1}): 3168, 1731, 1692, 1612, 1447, 1243, 1216, 1150, 1076, 1011, 938. HR-MS (ESI-TOF) *m*/*z* calcd for $C_{18}H_{10}N_3O_3Br$ $[M + H]^+$: 395.9985, found 395.9975.

2.2.5 4-(1-(6-Chloro-2-oxo-2*H*-chromen-3-yl)-1*H*-1,2,3-triazol-4-yl)benzaldehyde (1e). Beige solid (87%). Mp: 234–235 °C. ^{1}H NMR (300 MHz, DMSO-d_6, δ): 10.05 (s, 1H, HCO), 9.32 (s, 1H, H-9), 8.79 (s, 1H, H-4), 8.25 (d, 2H, $^3J = 8.2$, H-13), 8.11 (d, 1H, $^4J = 2.6$, H-5), 8.03 (d, 2H, $^3J = 8.2$, H-12) 7.80 (dd, 1H, $^4J = 2.6$, $^3J = 8.9$, H-7), 7.64 (d, 1H, $^3J = 8.9$, H-8). ^{13}C NMR (75.4 MHz, DMSO-d_6, δ): 193.1 (HCO), 155.7 (C-2), 151.4 (C-8a), 148.1 (C-10), 132.9 (C-7), 132.2 (C-14), 131.0 (C-11), 130.4 (C-4), 129.3 (C-5), 129.0 (C-13), 128.8 (C-12), 128.5 (C-3), 126.1 (C-9), 121.0 (C-6), 119.8 (C-8), 118.5 (C-4a). FT-IR (cm^{-1}): 3034, 1733, 1706, 1615, 1308, 1244, 1146, 1082, 1028, 954, 812. HR-MS (ESI-TOF) *m*/*z* calcd for $C_{18}H_{10}N_3O_3Cl$ $[M + H]^+$: 352.0489, found 352.0487.

2.2.6 4-(1-(8-ethoxy-2-oxo-2H-chromen-3-yl)-1H-1,2,3-triazol-4-yl)benzaldehyde (1f). Brown solid (84%). Mp: 231–232 °C. ^{1}H NMR (750 MHz, DMSO-d_6, δ): 10.04 (s, 1H, HCO), 9.28 (s, 1H, H-9), 8.79 (s, 1H, H-4), 8.23 (d, 2H, $^3J = 8.1$, H-13), 8.03 (d, 2H, $^3J = 8.1$, H-12), 7.49 (d, 1H, $^3J = 7.5$, H-5), 7.43 (d, 1H, $^3J = 7.5$, H-7), 7.40 (t, 1H, $^3J = 7.5$, H-6), 4.24 (q, 2H, $^3J = 6.9$, CH_2), 1.44 (t, 3H, $^3J = 6.9$, CH_3). ^{13}C NMR (188.6 MHz, DMSO-d_6, δ): 193.1 (HCO), 156.1 (C-2), 146.2 (C-10), 146.0 (C-8), 142.4(C-8a), 136.2 (C-11), 136.1 (C-4), 135.9 (C-14), 130.8 (C-13), 126.4 (C-12), 125.9 (C-6), 124.0 (C-9), 123.6 (C-3), 121.0 (C-7), 119.3 (C-4a), 116.6 (C-5), 65.0 (CH_2), 15.1 (CH_3). FT-IR (cm^{-1}): 3012, 1713, 1698, 1590, 1248, 1178, 1092, 950, 801. HR-MS (ESI-TOF) *m*/*z* calcd for $C_{20}H_{15}N_3O_4$ $[M + H]^+$: 362.1135, found 362.1130.

2.2.7 4-(1-(7-hydroxy-2-oxo-2*H*-chromen-3-yl)-1*H*-1,2,3-triazol-4-yl)benzaldehyde (1g). Brown crystalline solid (77%). Mp: >300 °C. ^{1}H NMR (750 MHz, DMSO-d_6, δ): 10.03 (s, 1H, HCO), 9.20 (s, 1H, H-9), 8.68 (s, 1H, H-4), 8.19 (d, 2H, $^3J = 8.1$, H-13), 8.01 (d, 2H, $^3J = 8.1$, H-12), 7.78 (d, 1H, $^3J = 7.6$, H-5), 6.91 (d, 1H, $^3J = 7.6$, H-6), 6.78 (s, 1H, H-8), δ OH not observed. ^{13}C NMR (188.6 MHz, DMSO-d_6, δ): 193.1 (HCO), 163.2 (C-7), 156.8 (C-2), 155.3 (C-8a), 145.9 (C-10), 137.4 (C-14), 136.1 (C-11), 136.0 (C-4), 131.6 (C-5), 130.8 (C-13), 126.3 (C-12), 124.2 (C-9), 119.5 (C-6), 114.9 (C-3), 110.8 (C-4a), 102.7 (C-8). FT-IR (cm^{-1}) 3162, 1730, 1706, 1610, 1392, 1243, 1169, 1021, 819. HR-MS (ESI-TOF) *m*/*z* calcd for $C_{18}H_{11}N_3O_4$ $[M + H]^+$: 334.0822, found 334.0822.

2.3 Computational methods

Density functional theory (DFT) calculations were performed using Gaussian 09w at the B3LYP/6-31 (d, p) level of theory in vacuum.[35] The frontier orbital energy calculations were performed in the optimized geometry. Linear transitions of absorption were estimated from the optimized molecular structures using time-dependent DFT (TDDFT) methods[36] at the BhandHLYP/6-31G (d, p) level of theory in vacuum for compounds **1a–g**. From the optimized structures, the first thirty electronic transitions were obtained. CPCM model in dichloromethane was used to mime solvent effects on electronic transitions.

2.4 Electrochemical characterization

Cyclic voltammetry (CV) measurements were recorded on a PARSAT® 2273 electrochemical instrument with a 3-electrode cell in a solution of 0.1 M of Bu_4NPF_6 in anhydrous acetonitrile at room temperature under nitrogen atmosphere with a scan rate of 50 mV s^{-1}. The working electrode was graphite deposited with **1a–g** films, which were formed by self-assembly on a graphite surface of 0.25 cm^2 using a saturated solution of the corresponding compound in CH_2Cl_2 as solvent. Platinum wire and saturated calomel electrode (SCE) were the auxiliary and reference electrodes, respectively. Ferrocene–ferrocenium (Fc/Fc^+) couple was chosen as internal standard. The energy levels of the frontier molecular orbitals (FMOs), E_H^{EQ} and $E_L{}^{EQ}$, as well as H → L gap, E_{HL}^{EQ}, electrochemical values were calculated as reported[37,38] using the following empirical equations: $E_H^{EQ} = -e(E_{onset(Ox)} + 4.4)$, $E_L^{EQ} = -e(E_{onset(Red)} + 4.4)$ and $E_g^{EQ} = -(E_H^{EQ} - E_L{}^{EQ})$, where $E_{onset(Ox)}$ and $E_{onset(Red)}$ are the oxidation and reduction potentials in the corresponding onsets (H = HOMO, L = LUMO).

2.5 Film resistivity measurements

Thin films of **1a–g** were deposited on glass slides from CH_2Cl_2 solutions. The thickness was measured with AMBIOS XP-100 Thickness Profilometer ($A = 1$ cm^2, thickness = 580–620 nm). The sheet resistivity measurements were performed with Signatone Pro-4 of LucasLabs, configured with inline four-point probe. Squared probes were used, the contact points were distanced such as: $S_{12} = S_{23} = S_{34} = S = 1$ mm.

3 Results and discussion

3.1 Synthesis and characterization

3-(4-Formylphenyl)-triazole functionalized coumarins **1a–g** were prepared *via* one pot reaction between four components, Scheme 1. The reaction requires an aldol condensation of a series of salicylaldehydes (**a–g**) with ethyl bromoacetate promoted by piperidine, coupled to a 1,3-Huisgen cycloaddition reaction between 4-ethynylbenzaldehyde, in the presence of sodium azide under mild reaction conditions (^{i}Pr–OH–DMF–H_2O, 80 °C) and using CuCN as catalyst (10% mol). The FPhTCs **1a–g** were isolated in moderate to high yields (75–97%) and high purity after short reaction times without the need of chromatographic purification. It is worth to note that the chemistry of triazole dyes, synthesized through click procedures, has been recently reviewed[39] where the use of CuCN as catalyst is scarce. Our group has demonstrated the

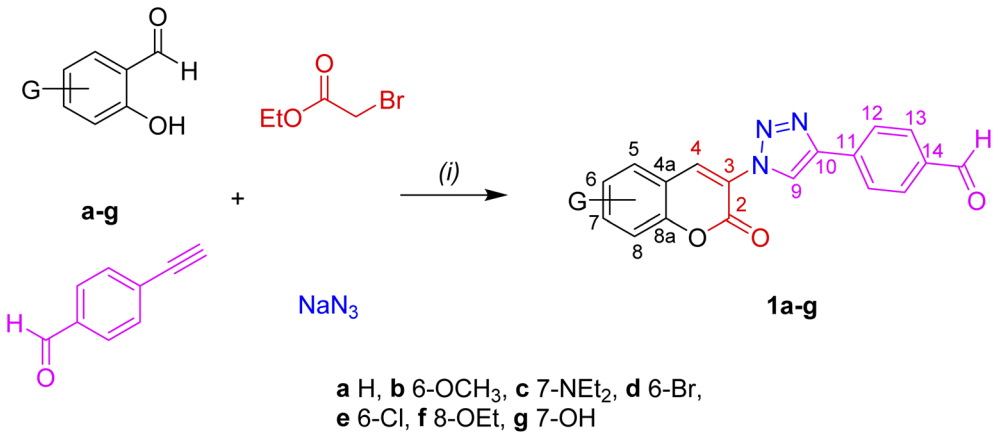

Scheme 1 Route of synthesis for FPhTC compounds **1a–g**. (*i*) ^{i}PrOH-DMF (3 : 1), piperidine, Et_3N, CuCN (10% mol), reflux.

applicability of CuCN to catalyze the formation of 1,4-disubstituted-1,2,3-triazoles from alkyl azides and mono-substituted acetylenes since CuCN is generated *in situ* by means of the NaCN reduction of $CuSO_4$.[40] It is worth to mention that the use of CuCN improves the yields in 10–20% compared to CuI. In addition, the aldehyde group in the 4-ethynylbenzaldehyde is not reactive enough to take part in the condensation reaction remaining intact in the final products for further functionalization.

Introduction of an electron donor group (EDG), such as –OMe in the *-meta* position to the formyl group in the salicylaldehyde, lead to the best performance to obtain 97% of **1b**. Good yields are also obtained with *m*-Br (93%) and *m*-Cl (87%) substituents compared with the *p*-NEt_2 (75%) or *p*-OH (77%) EDGs, the yields for all compounds are listed in Table S1.† Delocalization of the lone pairs from the *p*-EDGs is playing a key role in decreasing the electrophilic character of the salicylaldehyde involved in the formation of the coumarin ring. The ^{1}H-NMR spectra of conjugated FPhTCs **1a–g** show two characteristic signals in the δ 9.30–8.86 and 8.79–8.62 ranges, the former corresponding to the triazole ring proton (H-9) and the last to the vinyl proton on the coumarin heterocycle (H-4), in addition to the aldehyde proton singlet at $\delta \sim 10$.

3.2 Photophysical properties

The optical properties of **1a–g** were investigated by absorption-emission spectroscopy in solution and solid films. The corresponding data are summarized in Tables 1 and 2, respectively. The absorption spectra of **1a–g** in CH_2Cl_2 are depicted in Fig. 1(a), their absorption profiles show two absorption maxima centered at 306–275 nm (λ_1) and 421–327 nm (λ_2). The high energy band is attributed to π–π^* transitions of the 4-(1,2,3-triazolyl)formylphenyl fragment whereas the longer wave band is attributed to π–π^* transitions of the 3-(1,2,3-triazolyl) coumarin moiety. It is worth to mention that the 7-EDGs exert the largest bathochromic shift and strongly increase the intensity of λ_2 as the result of the coumarin polarization along the C3–C7 axis. This effect is more pronounced in compound **1c** than **1g** by 86 and 21 nm, as compared to **1a**, and has been attributed to the better donor properties of the 7-NEt_2 group than 7-OH. The optical band-gaps ($E_{g\text{-}opt}$) of **1a–g** show values between 3.25 to 2.68 eV, with absorptivity coefficients (ε_2) within the same order of magnitude ($\sim 10^4$ M^{-1} cm^{-1}). The emission spectra of **1a–g** in solution are shown in Fig. 1(b). All compounds exhibited fluorescence in solution at λ_{em} in the 473–419 nm range. As expected, the largest bathochromic shift ($\sim$48 nm) was exhibited by **1c** (7-NEt_2), as compared to unsubstituted **1a**, but the smallest Stokes shifts and the best

Table 1 Optical data of **1a–g** in CH_2Cl_2 solutions at room temperature

	λ_{abs}[a]/nm							
FPhTC	λ_1	λ_2	$\varepsilon_2/10^4$ M^{-1} cm^{-1} (% error)	$E_{g\text{-}opt}$/eV	λ_{em}[b]/nm	Stokes shift/cm^{-1}	Fluorescence[c]	Φ (CH_2Cl_2)
1a	297	335	2.41 (1.5)	3.17	425	6321	17 918	0.17
1b	301	362	1.42 (2.3)	2.98	443	5051	10 761	0.11
1c	275	421	2.87 (1.0)	2.68	473	2611	43 162	0.39
1d	289	345	1.23 (1.2)	3.12	436	6050	5 929	0.08
1e	296	353	1.68 (2.2)	3.17	436	5393	19 518	0.24
1f	306	327	2.73 (2.3)	3.25	451	8408	2 018	0.02
1g	297	356	2.87 (1.1)	3.07	419	4224	49 413	0.57

[a] Absorption in CH_2Cl_2 3.5×10^{-5} M. [b] Emission maximum in THF 10^{-6} M excited at the absorption maximum. [c] Measured from experimental emission spectra as area under the curve in area units.

Table 2 Optical data of **1a–g** in solid films at room temperature

FPhTC	$\lambda_{abs\text{-}film}$/nm[a]	$E_{g\text{-}opt}$ /eV	$\lambda_{em\text{-}film}$/nm[b]	Stokes shift/cm^{-1}	Fluorescence[c]
1a	283	2.82	458	13 502	38 239
1b	286	2.93	454	12 939	30 591
1c	296, 413[d]	2.63	525, 568	5 165	38 703
1d	296, 359[e]	2.92	449	11 512	11 534
1e	316	2.73	442	9 021	22 834
1f	289	3.17	452	12 478	3 065
1g	285	2.91	423	11 447	16 614

[a] Absorption of thin solid films. [b] Emission of thin solid film excited at the absorption maximum. [c] Measured from experimental emission spectra as area under the curve in area units. [d] λ_2. [e] Shoulder.

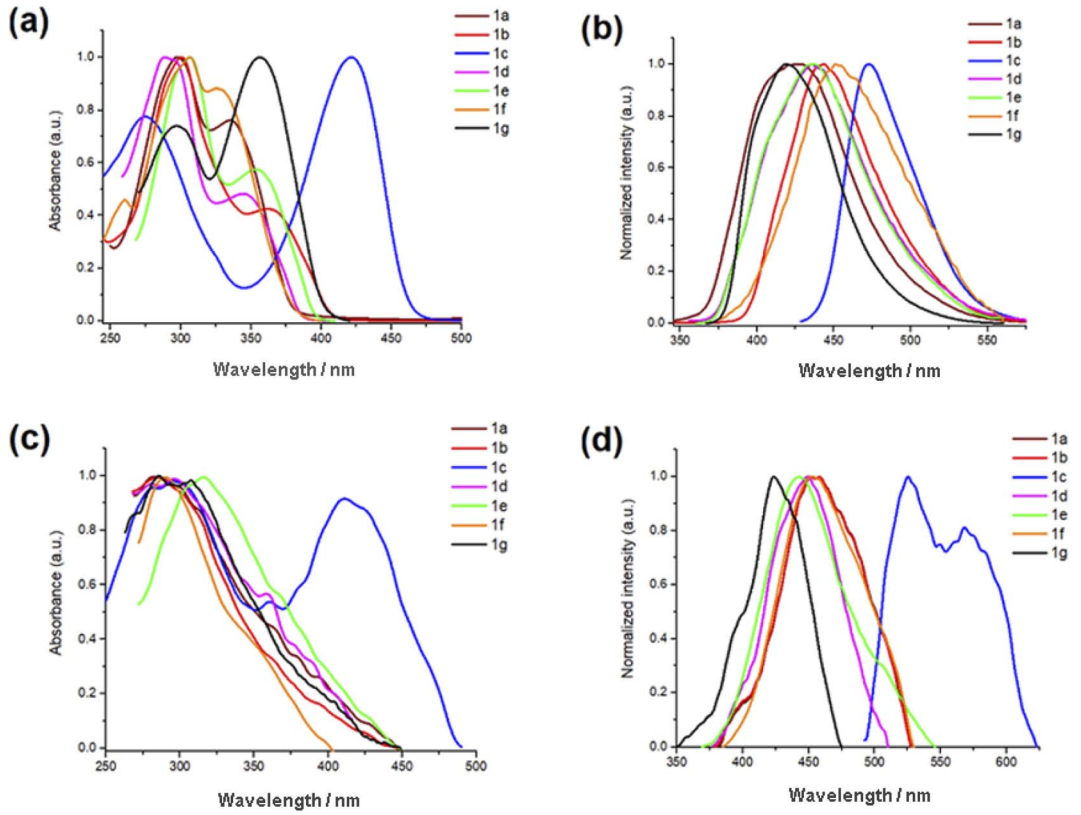

Fig. 1 Normalized absorption and emission spectra of PhTCs **1a–g**. (a) Absorption in CH_2Cl_2 solutions 3×10^{-5} M. (b) Emission in CH_2Cl_2 solutions 10^{-6} M. (c) Absorption and (d) emission in thin films formed after three submersions of 15 min in a 2×10^{-4} M in CH_2Cl_2 solutions.

fluorescence quantum yields (Φ) are shown by both **1c** (7-NEt$_2$) and **1g** (7-OH). These results revealed that the electronic push–pull system depends on the coumarin substituent. In comparison with other 3-(triazolyl)coumarin fluorophores,[22,26,41] compounds **1a–g** show similar Stokes shifts and quantum yields but smaller values than 4-(triazolyl)coumarin fluorophores.[18,21]

The absorption spectra of FPhTCs, in solid films, broaden to observe only one asymmetric band centered at short-wavelengths, except in **1c** whose absorption profile strongly resembles that in solution, Fig. 1(c). The blue shift of the absorption band implies less π-electrons available and/or shorter π-conjugated structures in the solid than in solution. This result indicates a diminution of the intramolecular electronic communication between the FPhT and coumarin moieties in all compounds in the ground state, except **1c**. This effect can be explained as the consequence of a fixed non-coplanar conformation between the two partners in the crystal network, in agreement with our previous study where the torsion angle between FPhT and coumarin fluorophores are in the 5.8–21.5° range.[27] Even though, the $E_{g\text{-}opt}$ values of **1a–g** are between 2.63 to 3.17 eV, slightly smaller than in solution. Furthermore, the λ_{em} maxima are red-shifted for all compounds, Fig. 1(d), generating a two-fold increase in the Stokes shift values compared to those in solution. Therefore, a major electronic redistribution in the solid state occurs prior to emission, probably due to the vibrational relaxation during

the charge transfer. The large Stokes shifts, the high absorption coefficients, fluorescence quantum yields, and emission in the solid state make FPhTCs **1a–g** good candidates for optoelectronic or imaging applications.[42]

The donor properties of azoles are well known,[43] then it can be rationalized that the triazole fragment behaves as the donor and the FPh fluorophore behaves as the acceptor, in contrast to the dual behavior shown by coumarin. The donor–acceptor (D–A) properties of coumarin are switched in/on depending upon the nature of the coumarin substituent,[44,45] and the physical state.[46,47] The proposed resonance structures **A**, **B** and **C** are depicted in Fig. 2. In solution, the coumarin fragment acts as the acceptor in the FPhTCs **1a,b,d–f**, to develop the resonance form **A**. The strong donor groups, 7-NEt_2 and 7-OH in **1c** and **1g**, favor the electronic delocalization of the triazole fragment into the FPh ring, developing the resonance structure **B**. It can be concluded that the triazole linker exerts a synergic effect, in compounds **1c** and **1g**, resulting in enhanced D–A interaction. The D properties of the triazole linker can be rationalized by a contribution from resonance structure **B** to the excited state, as previously observed for *N*-phenyl-triazoles.[48] In the solid, the FPhT moiety is twisted away from the coumarin plane interrupting the electronic communication between both moieties in all FPhTCs, leading to the resonance structures **C** in compounds **1a,b,d–f** and **B**-twisted in **1c**, which are proposed to contribute to the excited state. Fluorescence in crystals of slightly twisted 3-phenyl-coumarins have been observed to show dual solution and solid luminescences[47,49] as herein demonstrated for compounds **1a–g**.

3.3 Theoretical calculations

The structures of **1a–g** were optimized by DFT B3LYP/6-31G (d, p) level of theory in CH_2Cl_2. The computed geometry predicts an almost planar molecular structures with torsion angles near to 0° between triazole and coumarin, and FPh and triazole rings, in contrast with the measured values in analogous molecules (5.8–21.5°, T–C; and 1.6–18.1°, FPh-T),[27] a complete list of calculated torsion angles is in Table S2.† The theoretical absorption spectra of **1a–g**, obtained with BhandHLYP/6-31G (d, p), CPCM model in CH_2Cl_2, are in good correspondence with the experimental ones, Fig. 3(a), even though the predicted λ_{max} are shifted to the blue. Calculations were also performed in THF solution and in vacuum without significant changes. Visualization of the FMOs of the optimized structures of **1a**, **1c** and **1f** in CH_2Cl_2 is shown in Fig. 3(b), and the complete palette is shown in Fig. S22.† The lowest energy transitions, their oscillator strength (*f*) and their probable orbital nature are listed in Table 3, a complete list of the main transitions can be found in Tables S3.† Three electronic transitions are clearly defined, from them the red shifted corresponds to the electronic transition H → L in 81–93% and a small participation of H-1 → L in 11–13%, with oscillator strength values between 0.8 and 1.3. The HOMO is mainly delocalized over the FPhT moiety whereas the LUMO is centered on the coumarin fragment, as has been calculated in other coumarins.[50] In contrast, the localization of

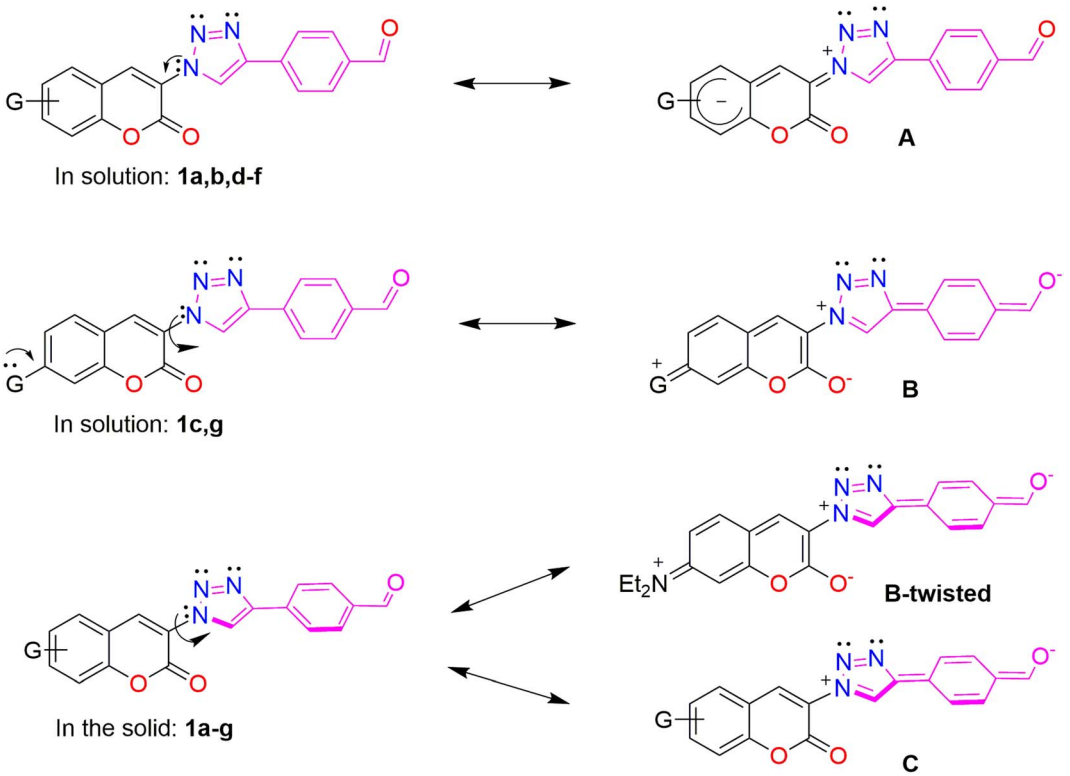

Fig. 2 Resonance structures showing the electronic delocalization and the D–A behavior of coumarin, FPh and triazole fragments.

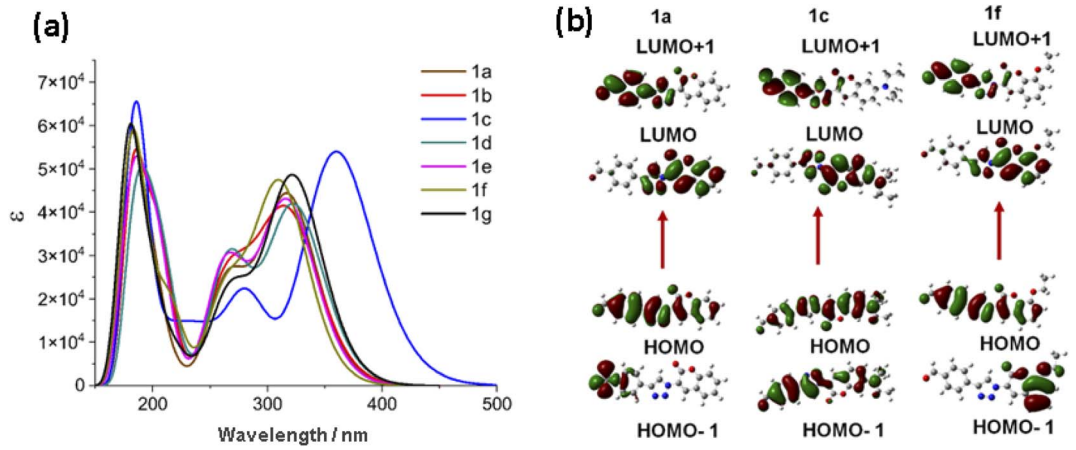

Fig. 3 (a) Theoretical absorption spectra obtained by TDDFT BhandHLYP/6-31G (d, p), CPCM solvent model (CH_2Cl_2) (b) Isosurfaces of the HOMO, LUMO, HOMO-1 and LUMO+1 orbitals of **1a**, **1c** and **1f**.

Table 3 Main electronic transitions obtained by BhandHLYP/6-31G (d, p), CPCM model in CH_2Cl_2

FPhTC	λ_{max}/nm	E/eV	OS (f)	MO/character	$E_{H\rightarrow L}$/eV
1a	318.48	3.8935	1.1	H → L (83%); H-1 → L (12%)	3.64
1b	322.64	3.8433	0.8	H → L (85%); H-4 → L (8%)	3.63
1c	360.19	3.4426	1.3	H → L (93%); H → L + 1 (2%)	3.49
1d	323.82	3.8293	1.0	H → L (82%); H-1 → L (11%)	3.54
1e	317.59	3.9044	1.0	H → L (81%); H-1 → L (13%)	3.54
1f	312.43	3.9689	1.1	H → L (81%), H-1 → L (11%)	3.72
1g	322.90	3.8402	1.2	H → L (90%); H-1 → L (5%)	3.66

the H-1 depends on the coumarin substitution, it is centered in the FPh fragment (**1a**, **1d**, **1e**), in the coumarin (**1f**) or in the whole molecule (**1b**, **1c**, **1g**). Their E_{HL}^{DFT} values are in the 3.72–3.49 eV range, larger than the experimental optical band gaps because of the predicted blue shift of the λ_{max}.

3.4 Electrochemical and film resistivity characterization

The electrochemical properties of **1a–g** were evaluated in solid films by cyclic voltammetry (CV). The electrochemical data are listed in Table 4 and the cyclic voltammograms are depicted in Fig. 4(a). The voltammograms are characterized by a quasi-reversible processes. In general, in the reduction zone the formation of π-radical anion is observed with $E_{onset(Red)}$ values ranging between −1.32 to −1.50 V. The formation of a π-radical cation, attributed to the triazole donor, is observed in the oxidation region. The $E_{onset(Ox)}$ values are in the 1.16–1.53 V range, Fig. S23.† The electrochemical energy of the HOMO (E_H^{EQ}) and LUMO (E_L^{EQ}) FMOs, were obtained from the oxidation and reduction potentials in the onset, respectively.[51] The electrochemical H → L gap (E_{HL}^{EQ}) mean value is of 2.79 ± 0.08 eV, therefore compounds **1a–g** are good prospects for semiconductor materials with attractive redox electrochemical properties. These results are in agreement with those experimentally measured by absorption spectroscopy in the solid state and smaller than those predicted by DFT computations. At last, thin films of the FPhTC compounds **1a–g** were deposited on glass slides, in order to measure their electric resistivity, Fig. 4(b). They show resistivity values between 10^4 to 10^5 Ω cm, Table S4.† in agreement with the expected values for semiconducting organic materials,[52] the best values are shown by

Table 4 Electrochemical properties from CV data and theoretical dipole moment of **1a–g**

FPhTC	$E_{onset(Red)}$/V	$E_{onset(Ox)}$/V	E_L^{EQ}/eV	E_H^{EQ}/eV	E_{HL}^{EQ}/eV	Dipole moment/D
1a	−1.32	1.45	−3.08	−5.85	2.77	8.0
1b	−1.32	1.43	−3.08	−5.83	2.75	10.0
1c	−1.46	1.16	−2.94	−5.56	2.62	12.7
1d	−1.4	1.41	−3.00	−5.81	2.81	6.2
1e	−1.40	1.42	−3.00	−5.82	2.82	6.8
1f	−1.35	1.53	−3.05	−5.93	2.88	10.2
1g	−1.50	1.39	−2.90	−5.79	2.89	9.7

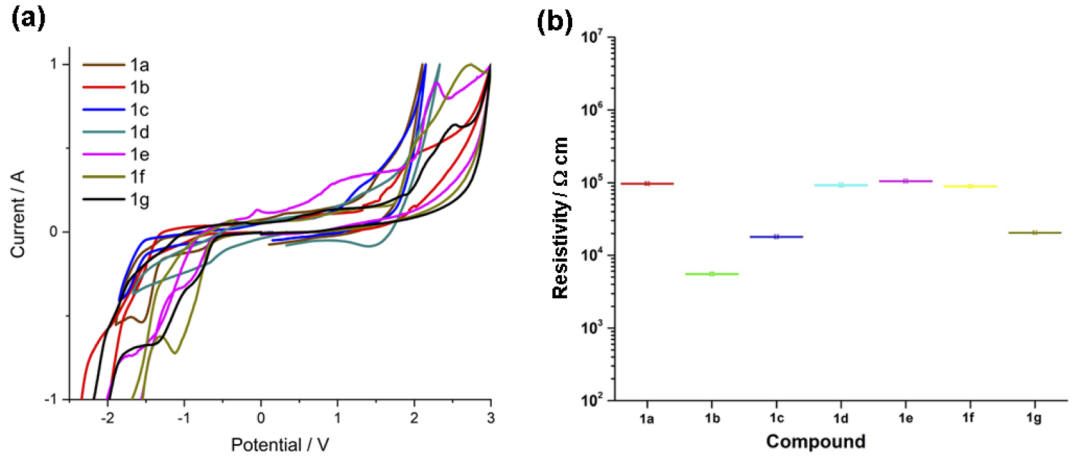

Fig. 4 (a) Voltammograms of **1a–1g** *vs.* SCE. (b) Comparison of resistivity values of **1a–g** in solid films.

compounds **1b**, **1c** and **1g**, substituted with ED groups and associated with large dipole moments, Table 4. Resistivity values agree with electrochemical H → L gap (E_{HL}^{EQ}).

3.5 Thermal stability

The thermal stability was established by thermogravimetry (TG) and differential scanning calorimetry (DSC) measurements performed under air. The thermograms of **1a–g** are displayed in Fig. 5. FPhTCs are thermally stable up to 225 °C, with the exception of compound **1c** whose thermal decomposition begins at ~200 °C. DSC analyses show that decomposition is a multistep process, in some cases (**1a**, **1b**, **1f**) an endothermic peak, associated with melting, is observed before decomposition occurs. Nevertheless, solid phase transitions were absent in all DSC measurements in Fig. S24–30.† These results make compounds **1a–g** in the range of thermal stability required for further applications.

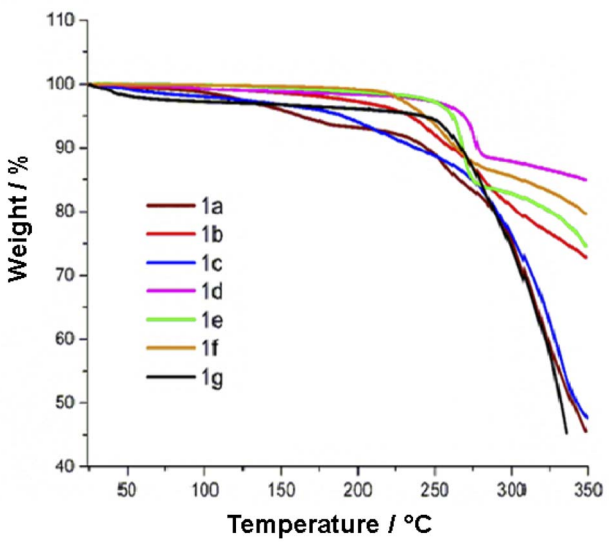

Fig. 5 Thermograms of compounds **1a–g** recorded under air.

4 Conclusion

Herein we present the synthesis, spectrochemical, electrochemical, photophysical and thermal characterization of 3-(4-formylphenyl)-triazole-coumarin hybrid chromophores (FPhTCs). The overall achievements indicate that they might be effective for the development of long wavelength emissive and white-light-emitting chromophores due to their large Stokes shifts, high absorption coefficients, fluorescence quantum yields, excellent thermal properties, small resistivity values, and small electrochemical band-gaps which make FPhTCs good candidates for optoelectronic or imaging applications. The rational design of coumarin derivatives functionalized with electron-acceptor groups is proposed in order to obtain potential molecules or promising scaffolds as violet-blue luminophores for optoelectronic applications. Also, for the rational design of precursors for the synthesis of higher molecular weight π-conjugated systems to take advantage of the intrinsic properties that coumarin-derived moieties exhibit.

Conflicts of interest

The authors declare no competing financial interest.

Author contributions

Conceptualization, funding acquisition and supervision, N. F., I. I. P.-M.; methodology, formal analysis, J. E. C.-P., O. J. H.-O., R. G.-A.; resources, validation, supervision, R. A. V.-G., H. L.-R.; writing–review & editing, I. I. P.-M. All the authors have read and agreed to the final version of the manuscript.

Acknowledgements

I. I. P.-M. gratefully acknowledges the financial support from CONACYT (grant 255354) and SIP-IPN. N. F. acknowledges the Faculty of Chemistry-UNAM (PAPIIT IN-222819 and PAIP 5000-9056) and CONACYT (A1-S7642). JEC-P thanks CONACYT and DGAPA, for the postdoctoral fellowship.

References

1 B. Fang, P. Li, J. Jiang, W. Du, L. Wang, H. Bai, B. Peng, X. Huang, Z. An, L. Li, X. Yang, L. Fu and W. Huang, *Coord. Chem. Rev.*, 2021, **440**, 213979.

2 Z. Yang, X. Fan, H. Li, X. Li, S. Li, Z. Zhang, H. Lin, J. Qian and J. Hua, *Chem.–Eur. J.*, 2021, **27**, 14240.

3 K. Pal, T. Dutta and A. L. Koner, *ACS Omega*, 2021, **6**, 28.

4 J. Han, S. Guo, H. Lu, S. Liu, Q. Zhao and W. Huang, *Adv. Opt. Mater.*, 2018, **6**, 1800538.

5 G. He, Organic Optoelectronic Materials, *Lect. Notes Chem.*, 2015, **91**, 241.

6 T. Yu, L. Liu, Z. Xie and Y. Ma, *Sci. China: Chem.*, 2015, **58**, 907.

7 M.-S. Wang and G.-C. Guo, *ChemComm*, 2016, **52**, 13194.

8 G. Jiang, Y. Song, X. Guo, D. Zhang and D. Zhu, *Adv. Mater.*, 2008, **20**, 2888.

9 R. M. Tomb, T. A. White, J. E. Coia, J. G. Anderson, S. J. MacGregor and M. MacLean, *Photochem. Photobiol.*, 2018, **94**, 445.

10 H. Zhang, Q. Luo, Y. Mao, Y. Zhao and T. Yu, *J. Photochem. Photobiol., A*, 2017, **346**, 10.

11 Y. Li, T. Yu, W. Su, Y. Wang, Y. Zhao and H. Zhang, Polycyclic aromatic hydrocarbon-bridged coumarin derivatives for organic light-emitting devices, *Arabian J. Chem.*, 2020, **13**, 4126.

12 G. Tian, Z. Zhang, H. Li, D. Li, X. Wang and C. Qin, *Crit. Rev. Anal. Chem.*, 2021, **51**, 565.

13 Y. Zhang, Y. Zhang, Y. Yue, J. Chao, F. Huo and C. Yin, *Sens. Actuators, B*, 2020, **320**, 128348.

14 V. S. Padalkar, S. B. Chemate, S. K. Lanke and N. Sekar, *J. Lumin.*, 2015, **168**, 114.

15 A. Tigreros and J. Portilla, *RSC Adv.*, 2020, **10**, 19693.

16 P. Kautny, D. Bader, B. Stöger, G. A. Reider, J. Fröhlich and D. Lumpi, *Chem.–Eur. J.*, 2016, **22**, 18887.

17 H. Guo, M. Fan, Z. Li, W. Tang and X. Duan, *Anal. Methods*, 2018, **10**, 5629.

18 P. Thasnim and D. Bahulayan, *New J. Chem.*, 2017, **41**, 13483.

19 E.-D. Chenot, J. C. Rodríguez-Domínguez, P. Hannewald, A. Comel and G. Kirsch, *J. Heterocycl. Chem.*, 2008, **45**, 1429.

20 J.-L. Xue, X.-P. He, J.-W. Yang, D.-T. Shi, C.-Y. Cheng, J. Xie, G.-R. Chen and K. Chen, *Carbohydr. Res.*, 2012, **363**, 38.

21 A. V. Nyuchev, E. A. Sharonova, N. A. Lenshina, A. S. Shavyrin, M. A. Lopatin, I. V. Balalaeva, I. P. Beletskaya and A. Y. Fedorov, *Tetrahedron Lett.*, 2011, **52**, 4196.

22 J. M. V. Ngororabanga, J. Du Plessis and N. Mama, *Sensors*, 2017, **17**, 1980.

23 N. Mama and A. Battison, *Arkivoc*, 2020, 59.

24 A. Bistrović, N. Stipaničev, T. Opačak-Bernardi, M. Jukić, S. Martinez, Lj. Glavaš-Obrovac and S. Raić-Malić, *New J. Chem.*, 2017, **41**, 7531.

25 K. Sivakumar, F. Xie, B. M. Cash, S. Long, H. N. Barnhill and Q. Wang, *Org. Lett.*, 2004, **6**, 4603.

26 X. He, R. Li, M. Xie, J. Duan, Q. Tang and Y. Shang, *New J. Chem.*, 2020, **44**, 12266.

27 J. E. de la Cerda-Pedro, R. Arcos-Ramos, M. Maldonado-Domínguez, S. Rojas-Lima, M. Romero-Ávila, M. P. Carreón-Castro, R. Santillan, N. Farfán and H. López-Ruiz, *CrystEngComm*, 2016, **18**, 5562.

28 R. Arcos-Ramos, M. Maldonado-Domínguez, J. Ordóñez-Hernández, M. Romero-Ávila, N. Farfán and M. P. Carreón-Castro, *J. Mol. Struct.*, 2016, **1130**, 914.

29 T. Hirano, H. Kubo, T. Shiraishi, K. Hiromoto, T. Fujiwara and H. Kagechika, *Tetrahedron Lett.*, 2012, **53**, 5916–5919.

30 J. L. Vázquez, I. Velazco-Cabral, E. Alvarado-Méndez, M. Trejo-Durán, M. Flores-Alamo, E. Peña-Cabrera, M. A. García-Revilla and M. A. Vázquez, *Phys. Chem. Chem. Phys.*, 2021, **23**, 22466–22475.

31 C. Zhong, J. Gao, Y. Cui, T. Li and L. Han, *J. Power Sources*, 2015, **273**, 831–838.

32 L. Han, R. Kang, X. Zu, Y. Cui and J. Gao, *Photochem. Photobiol. Sci.*, 2015, **14**, 2046–2053.

33 D. Cao, Z. Liu, P. Verwilst, S. Koo, P. Jangjili, J. S. Kim and W. Lin, *Chem. Rev.*, 2019, **119**, 10403–10519.

34 T. S. Reddy, J. Hwang and M. S. Choi, *Dyes Pigm.*, 2018, **158**, 412–419.

35 M. J. Frisch, G. W. Trucks, H. B. Schlegel, G. E. Scuseria, M. A. Robb, J. R. Cheeseman, G. Scalmani, V. Barone, B. Mennucci, G. A. Petersson, H. Nakatsuji, M. Caricato, X. Li, H. P. Hratchian, A. F. Izmaylov, J. Bloino, G. Zheng, J. L. Sonnenberg, M. Hada, M. Ehara, K. Toyota, R. Fukuda, J. Hasegawa, M. Ishida, T. Nakajima, Y. Honda, O. Kitao, H. Nakai, T. Vreven, J. A. Montgomery Jr, J. E. Peralta, F. Ogliaro, M. Bearpark, J. J. Heyd, E. Brothers, K. N. Kudin, V. N. Staroverov, R. Kobayashi, J. Normand, K. Raghavachari, A. Rendell, J. C. Burant, S. S. Iyengar, J. Tomasi, M. Cossi, N. Rega, J. M. Millam, M. Klene, J. E. Knox, J. B. Cross, V. Bakken, C. Adamo, J. Jaramillo, R. Gomperts, R. E. Stratmann, O. Yazyev, A. J. Austin, R. Cammi, C. Pomelli, J. W. Ochterski, R. L. Martin, K. Morokuma, V. G. Zakrzewski, G. A. Voth, P. Salvador, J. J. Dannenberg, S. Dapprich, A. D. Daniels, O. Farkas, J. B. Foresman, J. V. Ortiz, J. Cioslowski and D. J. Fox, *Gaussian 09, Revision A.02*, Gaussian, Inc., Wallingford CT, 2009.

36 C. Adamo and D. Jacquemin, *Chem. Soc. Rev.*, 2013, **42**, 845.

37 C. M. Cardona, W. Li, A. E. Kaifer, D. Stockdale and G. C. Bazan, *Adv. Mater.*, 2011, **23**, 2367.

38 J. Sworakowski, *Synth. Met.*, 2018, **235**, 125.

39 D. Brunel and F. Dumur, Recent advances in organic dyes and fluorophores comprising a 1,2,3-triazole moiety, *New J. Chem.*, 2020, **44**, 3546–3561.

40 J. E. de la Cerda-Pedro, Y. A. Amador-Sánchez, M. Cortés-Hernández, J. Pérez-Pérez, S. Rojas-Lima and H. López-Ruiz, *Heterocycles*, 2014, **89**, 27–41.

41 A. Matta, M. Gupta, Y. Kumar, T. Taniike, J. Van der Eycken and B. K. Singh, *ChemistrySelect*, 2018, **3**, 10815.

42 M. Paramasivam and S. Kanvah, *J. Phys. Chem. C*, 2016, **120**, 10757.

43 Y. Zhang, X. Zheng, L. Zhang, Z. Yang, L. Chen, L. Wang, S. Liu and Z. Xie, *Org. Biomol. Chem.*, 2020, **18**, 707–714.

44 Y.-F. Sun, S.-H. Xu, R.-T. Wu, Z.-Y. Wang, Z.-B. Zheng, J.-K. Li and Y.-P. Cui, *Dyes Pigm.*, 2010, **87**, 109.
45 C. Ranjith, K. K. Vijayan, V. K. Praveen and N. S. Saleesh Kumar, *Spectrochim. Acta, Part A*, 2010, **75**, 1610–1616.
46 C. G. Hamaker and C. S. McCully, 3-Acetyl-7-(diethylamino) coumarin, *Acta Crystallogr., Sect. E: Struct. Rep. Online*, 2006, **62**, o2072–o2074.
47 K. Kanji, M. Taisuke, I. Keiko, T. Haruko and T. Hajime, *Heterocycles*, 2012, **84**, 315.
48 P. Kautny, D. Bader, B. Stöger, G. A. Reider, J. Fröhlich and D. Lumpi, *Chem.–Eur. J.*, 2016, **22**, 1.
49 Y. Sun, T. Wu, F. Zhang, R. Zhang, M. Wu, Y. Wu, X. Liang, K. Guo and J. Li, *Dyes Pigm.*, 2018, **149**, 73.
50 M. N. Kumbar, M. S. Sannaikar, S. K. J. Shaikh, A. A. Kamble, M. N. Wari, S. R. Inamdar, Q. Qiao, B. N. Revanna, M. Madegowda, J. P. Dasappa and R. R. Kamble, *Photochem. Photobiol.*, 2018, **94**, 261.
51 T. Johansson, W. Mammo, M. Svensson, M. R. Andersson and O. Inganäs, *J. Mater. Chem.*, 2003, **13**, 1316.
52 D. Ho, R. Ozdemir, H. Kim, T. Earmme, H. Usta and C. Kim, *ChemPlusChem*, 2019, **84**, 18–37.